Available online at www.sciencedirect.com

ScienceDirect

Ceramics International 40 (2014) 1717–1722

CERAMICS INTERNATIONAL

www.elsevier.com/locate/ceramint

Synthesis and characterization of lead zirconate titanate (PZT) obtained by two chemical methods

C.A. Oliveira*, E. Longo, J.A. Varela, M.A. Zaghete

Interdisciplinary Laboratory of Electrochemistry and Ceramics, Institute of Chemistry, São Paulo State University, Araraquara, SP, 14800-900, Brazil

Received 6 June 2013; received in revised form 11 July 2013; accepted 12 July 2013
Available online 21 July 2013

Abstract

Lead zirconate titanate (PZT) was synthesized at the ratio of Zr/Ti = 52/48 using two synthesis methods: the polymeric precursor method (PPM) and the microwave-assisted hydrothermal method (MAHM). The synthesized materials were characterized by X-ray diffraction (XRD), scanning electron microscopy (SEM), particle size distribution by sedimentation, hysteresis measurements and photoluminescence (PL). The results showed that PZT powders are composed of tetragonal and rhombohedral phases. Different particle sizes and morphologies were obtained depending upon the synthesis method. From the hysteresis loop verified that PZT powders synthesized by the PPM have a typical loop of ferroelectric material and are more influenced by spatial charges while particles synthesized by the MAHM have a hysteresis loop similar to paraelectric material and are less influenced by spatial charges. Both samples showed PL behavior in the green region (525 nm) whereas the sample synthesized by the PPM showed higher intensity in spectra.

Keywords: D. PZT; Polymeric precursor method; Microwave-assisted hydrothermal method; Ferroelectrics

1. Introduction

Perovskite ceramics based on lead represent the main class of ferroelectric materials used commercially in the form of multilayer capacitors, piezoelectric transducers, pyroelectric detectors and optical sensors [1–3]. Among these ceramics, PZT is the most efficient and widely applied material [4,5]. These ceramics properties are strongly influenced by the density and microstructure which depend upon the procedure of synthesis and the powder processing [6]. Furthermore, the morphotropic phase boundary (MPB) [7] is an essential parameter to be considered because in this region tetragonal and rhombohedral phases coexist, and consequently the properties of these materials are improved (e.g., piezoelectric properties).

A PZT perovskite structure is distorted below 350 °C [8] (Curie temperature). When this structure has Zr^{4+} in position B (the center of the unit cell), the $PbZrO_3$ rhombohedral phase is evident. However, when Ti^{4+} occupies the B site of structure, the tetragonal phase of $PbTiO_3$ appears [9]. Both phases are ferroelectric and consequently exhibit spontaneous polarization [6,10]. The position of charge centers in the unit cell is crucial because in a polarizable material, the centers can be shifted relative to each other which results in a charge-induced dipole in the unit cell that produces characteristic ferroelectricity. When centers of positive and negative charges are at different positions within the unit cell in the absence of any charges and have a permanent dipole, the cell has spontaneous polarization [11]. In ferroelectric materials, the spontaneous polarization can be reversed by applying an electric field (the coercive field) (Ec). For higher fields which extend to the saturation polarization (Ps) and upon removal of the applied field, the polarization does not return to the null value. This phenomenon is defined as remanent polarization (Pr), and it is represented by the hysteresis loop [6].

PZT can be synthesized by different methods, and different morphologies can be obtained [12–15]. The PPM is often used

*Correspondence to: Interdisciplinary Laboratory of Electrochemistry and Ceramics, Institute of Chemistry, São Paulo State University—UNESP, Rua Prof. Francisco Degni 55, Quitandinha, P.O. Box 355, CEP, 14800-900, Araraquara, São Paulo, Brazil. Tel.: +55 16 3301 9828; fax: +55 16 3322 0015.
E-mail address: cibeleestr@gmail.com (C.A. Oliveira).

0272-8842/$ - see front matter © 2013 Elsevier Ltd and Techna Group S.r.l. All rights reserved.
http://dx.doi.org/10.1016/j.ceramint.2013.07.068

to synthesize perovskites, particularly the PZT [15,16]. This method promotes the polyesterification of cation chelates which form a resin of high viscosity and decrease the cation segregation during thermal decomposition [17]. However, in the fabrication of PZT ceramics, PbO volatility at high temperatures can occur which causes a fluctuation in the PZT composition. Usually an excess precursor which contains lead is used to correct this loss [4,18]. Today, another method which is commonly used to obtain these materials is the MAHM; it has been increasingly reported in the literature. This method has shown advantages such as lower energy consumption, a low temperature, a rapid heating process due to the direct interaction of radiation with water as well as a consequent acceleration of the crystallization process [19,20]. Several materials with different structures have been synthesized by the MAHM. Moura et al. synthesized ZnO with a flower-like shape [18]; Volanti et al. obtained CuO with sea urchin-like morphology [21]; and Teixeira et al. obtained PZT plate-like structures [22].

This study compares the influence of both methods on PZT powders characteristics, especially their ferroelectric and PL properties. The materials obtained in each synthesis also were characterized by XRD, SEM and particle size distribution. The best response of these powders relative to each other was evaluated from measurements.

2. Experimental procedure

2.1. Synthesis methods

Powders of $Pb(Zr_{0,52}Ti_{0,48})O_3$ (PZT) have been synthesized by the PPM and by the MAHM. The reagents used were: $Pb(NO_3)_2$ (Mallinckrodt; 99.7%), $ZrOCl_2 \cdot 8H_2O$ (Merck; 99.95%), TiO_2 (Vetec; 99.8%.), KOH (JT Baker; 87.2%), ethylene glycol (Aldrich; 99.5%), standard solutions of zirconium and titanium citrates and citric acid (Synth; 99.5%).

2.1.1. Synthesis by PPM

For this synthesis, a solution of zirconium and titanium citrates with known concentrations was used to prepare PZT powders in the ratio Zr/Ti of 52/48 [18]. This mixture was homogenized with constant stirring and heating (approximately at 90 °C) [17]. Due loss of organic matter in this method, an excess quantity (5%) of aqueous solution of Pb $(NO_3)_2$ was added to assure the stoichiometry, followed by citric acid. A clear solution was obtained, and ethylene glycol was added for the formation of a polyester. The molar ratio of lead:citric acid:ethylene glycol was 1:4:16 mol. Then the polyester was calcined at 400 °C to eliminate organic matter, and the resulting material was heat-treated at 600, 700 and 800 °C for 3 h.

2.1.2. Synthesis by MHAM

For this synthesis, a commercial microwave furnace (MARCH-CEM, USA) was used operating in a frequency of 2.45 GHz and 600 W. An aqueous suspension containing Pb $(NO_3)_2$, $ZrOCl_2 \cdot 8H_2O$ and TiO_2 was prepared, and a solution of KOH (1.8 mol L^{-1}) was added which resulted in a final concentration of 0.31 mol/L PZT. This precursor suspension was maintained at room temperature under constant stirring and was completely solubilized in the middle of the reaction with the assistance of the pressure and control temperature provided by microwave furnace. The KOH is a mineralization agent, which assists the reactants mass transport during the formation of seeds in the crystallization process and it also contributes to the crystal nucleation and the growth process, resulting in accelerating the reaction. Approximately 30 mL of this suspension was placed in a Teflon vessel with a capacity of 90 mL. The fill to 30% of the Teflon vessel volume ensured maximum pressure and efficiency. The Teflon vessel was sealed and placed in the microwave furnace and heated at 180 °C for 2 h. After synthesis, the light yellow precipitate was formed which is separated from the residual solution by centrifugation and washed with distilled water until a neutral pH was obtained; then it was dried at room temperature.

2.2. Characterizations

The materials were characterized by XRD (Rigaku, model D/Max-2500/PC) using CuKα radiation in the 2θ range from 20° to 80° with 0.02°/min, FE-SEM (JEOL, JSM-7500F). The particle size distribution of PZT powders was analyzed by sedimentation velocity centrifugation using an X-ray beam (X-ray Disc Centrifuge System Model BI-XDCW Particle Sizer Analizer). PZT powders were compacted in the form of pellets with uniaxial pressure of 27.6 MPa then isostatic pressure of 210 MPa. After this process the samples were placed in alumina boat and PbO powder was added in the amount of 5% of the weight of sample. The alumina boat was sealed with alumina paste to prevent the loss of lead by volatilization, and placed in a tubular furnace at 1200 °C for 3 h and heating rate of 10 °C/min.

After sintering, the pellets were weighed, and the diameter and thickness were measured. Then they were polished to calculate the relative density of the samples from the theoretical density. For hysteresis measurements (Equipment Radiant Technology RT6000 HVA using an amplifier with the maximum potential difference of 4000 V), an electric field of 3 MV/m was applied to the pellets (with thickness around 1.0 mm) at a constant frequency of 10 Hz. PL spectra were collected with a Thermal Jarrel-Ash Monospec 27 monochromator and a Hamamatsu R446 photomultiplier. The 350 nm exciting wavelength of a krypton ion laser (Coherent Innova) was used on the pellets, with the nominal output power of the laser maintained at 550 mW.

3. Results and discussion

Fig. 1 shows XRD patterns of the powders obtained by the PPM and calcined at different temperatures and by MAHM. XRD pattern peaks can be consistently indexed by the tetragonal structure (card JCPDS #33-0784) and also by the rhombohedral structure of the PZT (card JCPDS #73-2022). This result was expected because the molar ratio of

Zr/Ti (52/48) used in this work is within the morphotropic phase boundary [23] which ensures the coexistence of the two crystalline structures of PZT. Also, XRD pattern powder peaks synthesized by the PPM become better defined with an increase in the calcination temperature which indicates an increase in crystallinity of these materials.

Fig. 2 shows FE-SEM images of PZT powders obtained by PPM calcinated at different temperatures (see Fig. 2a–c) and by MAHM (see Fig. 2d). Note that the powder prepared by PPM is composed of micro-sized rounded particles; this structure forms large agglomerates. In addition, the size of this particle increases with an increase in the calcination temperature, but agglomerates have no significant variation in size. On the other hand, the powder prepared by the MAHM is composed of micro-sized cubes, and these structures do not form large agglomerates because they are not subjected to the calcination process.

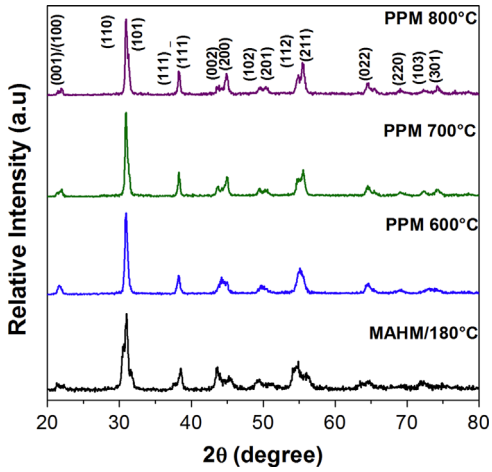

Fig. 1. XRD patterns of PZT powders obtained by the PPM and calcined at 600, 700 and 800 °C and by MAHM at 180 °C/2 h.

Powders obtained by the two synthesis methods were analyzed according to the particle size distribution. Fig. 3a–c shows the particle size distribution histogram of PZT powders synthesized by the PPM and calcinated at different temperatures. This analysis confirms that approximately 64% of particle sizes range from 1.1 to 1.7 μm, 81% of the particle sizes range from 1.25 to 1.75 and 58% of the particle sizes range from 1.3 to 1.7 μm at the calcination temperatures of 600, 700, and 800 °C, respectively. Fig. 3d is associated with PZT powders synthesized by the MAHM. About 80% of the particle sizes are between 1.25 and 3.25 μm. However, as viewed by FE-SEM (see Fig. 2a–d), the particles were agglomerated, so the size range obtained is related to the particle agglomerates and not isolated particles. The agglomerate size range has no significant variation according to the temperature increase which occurs because the temperature increase promotes the growth of particle sizes and not agglomerate sizes [24].

As the ferroelectric property is related to the density of the material, the PZT powder density obtained by the two synthesis processes was investigated. Table 1 shows the green density and the density after the sintering process. These data refer to the average of three samples made for each synthesis method. The green powder density of both synthesis methods are similar (approximately 60% of pure PZT found in the

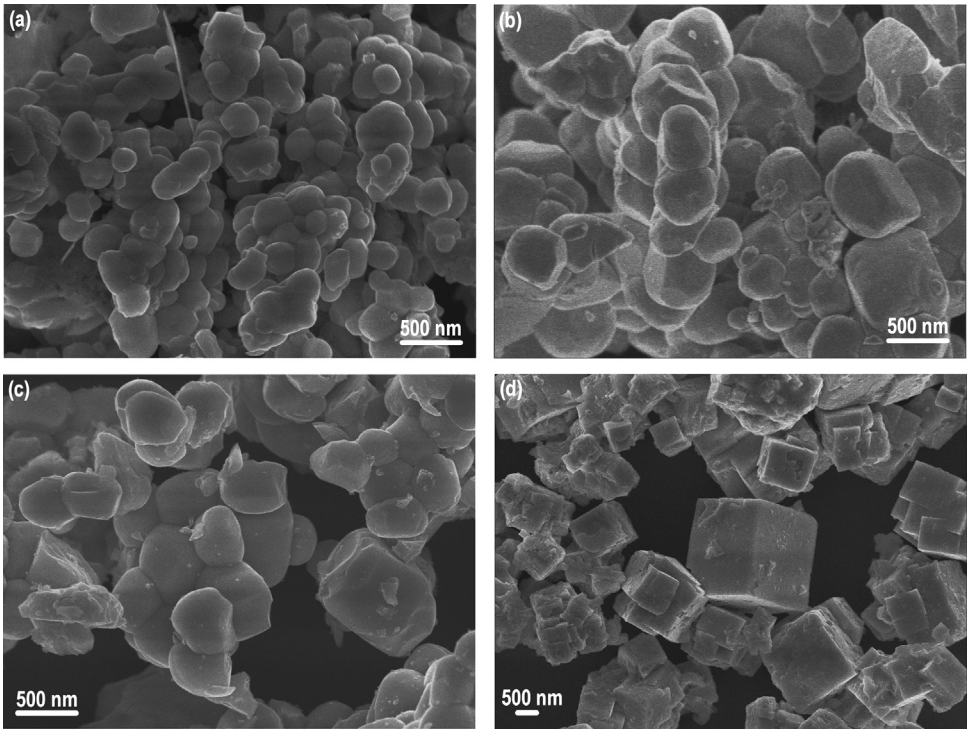

Fig. 2. FE-SEM of PZT powders synthesized by the PPM and calcined at different temperatures: (a) 600; (b) 700; (c) 800 °C; and (d) PZT powder synthesized by the MAHM concentration of 0.31 mol L^{-1} at 180 °C for 2 h.

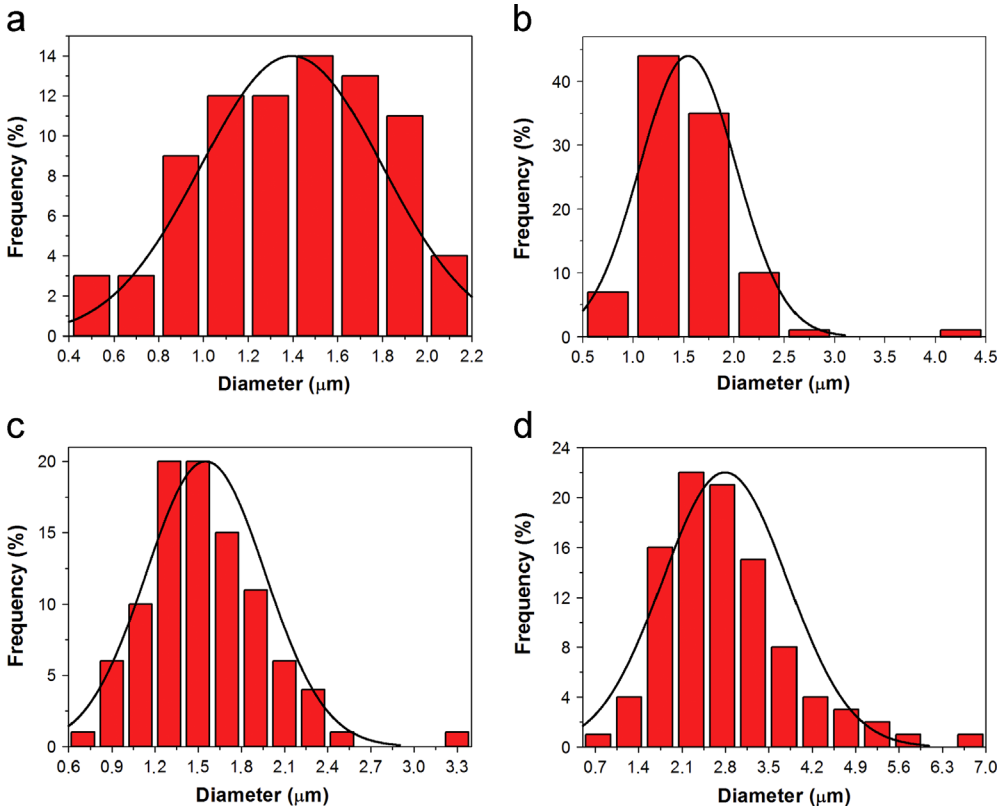

Fig. 3. Particle size distribution histograms of PZT powder obtained by the PPM with calcination temperatures of: (a) 600; (b) 700; and (c) 800 °C for 3 h. In the (d) histogram of PZT particle size distribution obtained by the MAHM at 180 °C for 2 h.

Table 1
Green density of PZT pellets and density after sintering.

Sample	Green density (g/cm^3) and (%)	Density after sintering (g/cm^3) and (%)	Mass loss (%)
PZT (PPM)	**4.81→60.9**	**7.20→91.2**	**5.8**
PZT (MAHM)	**4.42→56.0**	**7.21→91.3**	**2.9**

literature—7.9 g/cm^3) [25]. The same result occurs after the synthesis process (approximately 91% of theoretical density) (see Table 1).

Fig. 4 shows hysteresis loops obtained for the PZT powders by different synthesis methods. Considering that at low frequencies the contribution of spatial charges are visible, hysteresis measurements were performed at 10 Hz to investigate the influence of spatial charges on ferroelectric effects. Note that powders prepared by the PPM present a typical ferroelectric material loop and show remanent polarization (P_r) of 7.2 $\mu C/cm^2$ (see Fig. 4a) while for the powders prepared by the MAHM, reveal a characteristic loop of paraelectric materials (see Fig. 4b) and P_r cannot be observed. These results can be related to the spatial charges contribution for ferroelectric effect due to a smaller defect concentration on PZT powders prepared by the MAHM which we believe is consequence of the morphological influence obtained by this method.

Fig. 5 shows PL spectra at room temperature obtained for PZT powders synthesized by the PPM and the MAHM after excitation with a 350 nm laser light. A broad PL emission with the maximum at around 525 nm is verified. The higher intensity is for PZT powders prepared by the PPM in relation to the samples prepared by the MAHM. The lower PL of samples obtained by MAHM indicates that it is more ordered. Although the powders synthesized by both the methods are in the same phase, PZT structures obtained by the MAHM are more symmetrical than PZT structures obtained by the PPM, and consequently the PL intensity is lower.

The order can be related to the presence of ideal $[PbO_{12}]_o^x$, $[ZrO_6]_o^x$ and $[TiO_6]_o^x$ clusters or $[PbO_{12}]_o'$, $[ZrO_6]_o'$ and $[TiO_6]_o'$ electron polaron while disorder can be related to presence defective $[PbO_8]_d^x$ or $[PbO_7V_o^x]$, $[ZrO_6]_d^x$ or $[ZrO_5V_o^x]_d$ and $[TiO_6]_d^x$ or $[TiO_5V_o^x]$ clusters [26]. More recently, the cluster-to-cluster charge transfer (CCCT) process in a crystal containing more than one kind of cluster is characterized by excitations involving electronic transitions from one cluster to another cluster. The vacancy left behind by the electron polaron in an otherwise ideal cluster is termed a "hole polaron" which has all the attributes of an electron polaron except for being positively

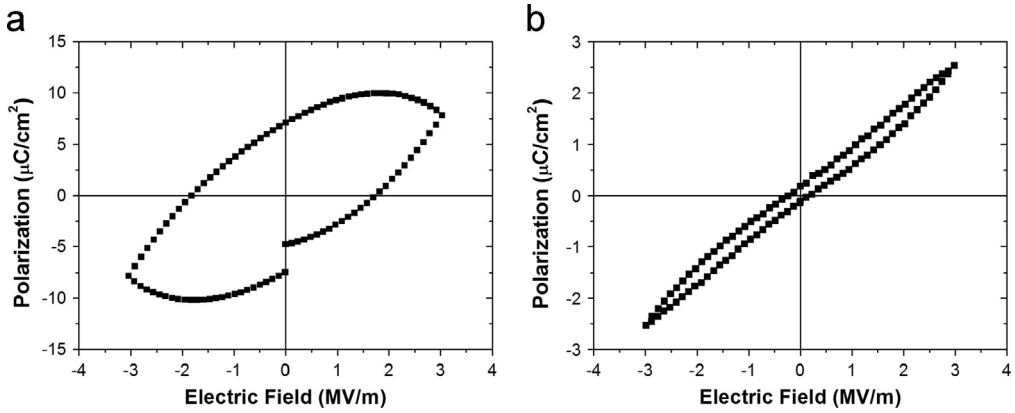

Fig. 4. *P–E* hysteresis loops for PZT. In (a) PZT pellet obtained by PPM and (b) PZT pellet obtained by MAH.

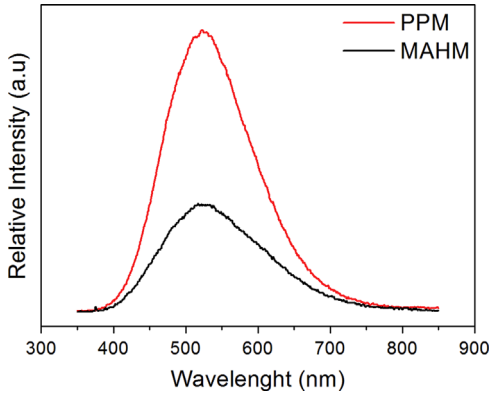

Fig. 5. PL spectra at room temperature of PZT powders obtained by the PPM and the MAHM.

charged, and hence there is a coulomb attraction between the electron/hole.

The CCCT process provides direct insight into charge carrier dynamics in materials. Hole polaron trap states are localized at oxygen anions in both bulk and surface, oxygen vacancies in a disordered structure with $[PbO_8]_o^x/[PbO_7V_o^x]$, $[ZrO_6]_o^x/[ZrO_5V_o^x]$, and $[TiO_6]_o^x/[TiO_5V_o^x]$ complex clusters [27] are hole trapping centers according to the following equations:

$$[PbO_8]_o^x + [PbO_7V_o^x] \rightarrow [PbO_8]_o' + [PbO_7V_o^\bullet] \quad (1)$$

$$[PbO_8]_o^x + [PbO_7V_o^\bullet] \rightarrow [PbO_8]_o' + [PbO_7V_o^{\bullet\bullet}] \quad (2)$$

$$[ZrO_6]_o^x + [ZrO_5V_o^x] \rightarrow [ZrO_6]_o' + [ZrO_5V_o^\bullet] \quad (3)$$

$$[ZrO_6]_o^x + [ZrO_5V_o^\bullet] \rightarrow [ZrO_6]_o' + [ZrO_5V_o^{\bullet\bullet}] \quad (4)$$

$$[TiO_6]_o^x + [TiO_5V_o^x] \rightarrow [TiO_6]_o' + [TiO_5V_o^\bullet] \quad (5)$$

$$[TiO_6]_o^x + [TiO_5V_o^\bullet] \rightarrow [TiO_6]_o' + [TiO_5V_o^{\bullet\bullet}] \quad (6)$$

Structural and electronic reconstructions of all possible combinations of clusters belonging to a specific crystal are essential for the understanding of the CCCT process and its influence on the PL and on ferroelectric effects (see Fig. 4b); as the system evolves to a higher structural order, there is a decrease in defect densities which is caused by the transformation of a $V_o^{\bullet\bullet}$ to $V_o^\bullet$ and subsequently the V_o^x oxygen vacancy in clusters [26] charge redistribution may promote a electron–hole recombination of localized excitons.

4. Conclusions

In this study, the influence of the synthesis method on morphology and on ferroelectric and PL properties of PZT powders was observed. XRD patterns confirm that PZT phases co-exist in the morphotropic phase boundary with different synthesis methods. FE-SEM images showed that particles with round and cubic forms were obtained by PPM and the MAHM, respectively.

Spatial charges have more influence on powders obtained by the PPM as verified by the formation of hysteresis loops that look round. PL spectra measurements verified a higher intensity in powders synthesized by the PPM; powders obtained by the MAHM were more ordained and contributed to low emission spectra. However, in both synthesis methods, powders show intense PL spectra in the green region (around 525 nm). The influence of the synthesis method on the formation of defects is confirmed by PL spectra and can also be correlated with hysteresis loop measurements. The two techniques complement each other and contribute to the understanding of phenomena related to the defect density and the existence of spatial charges in these materials.

Acknowledgments

The authors thank the Institute of Chemistry at the Unesp of Araraquara and its infrastructure for supporting this work. FE-SEM facilities were provided by the IQ-UNESP. We also thank the National Council for Scientific and Technological Development, CNPq, for financing this research.

References

[1] T. Morita, Piezoelectric materials synthesized by the hydrothermal method and their applications, Materials 3 (2010) 5236–5245.
[2] G.H. Haertling, Ferroelectric ceramics: history and technology, Journal of the American Chemical Society 82 (1999) 797–818.

[3] S.F. Wang, Y.R. Wang, T. Mahalingam, J.P. Chu, K.U. Lin, Characterization of hydrothermally synthesized lead zirconate titanate (PZT) ceramics, Materials Chemistry and Physics 87 (2004) 53–58.
[4] X.Y. Zhang, X. Zhao, C.W. Lai, J. Wang, X.G. Tang, J.Y. Dai, Synthesis and piezoresponse of highly ordered $Pb(Zr_{0.53}Ti_{0.47})O_3$ nanowire arrays, Applied Physics Letters 85 (2004) 4190–4192.
[5] G. Xu, W.J. Weng, H.X. Yao, P.Y. Du, G.R. Han, Low temperature synthesis of lead zirconate titanate powder by hydroxide co-precipitation, Microelectronic Engineering 66 (2003) 568–573.
[6] M. Cerqueira, R.S. Nasar, E. Longo, J.A. Varela, A. Beltran, R. Llusar, J. Andres, Piezoelectric behaviour of PZT doped with calcium: a combined experimental and theoretical study, Journal of Materials Science 32 (1997) 2381–2386.
[7] C.A. Randall, N. Kim, J.-P. Kucera, W. Cao, T.R. Shrout, Intrinsic and extrinsic size effects in fine-grained morphotropic-phase-boundary lead zirconate titanate ceramics, Journal of the American Chemical Society 81 (1998) 677–688.
[8] G. Xu, W. Jiang, M. Qian, X.X. Chen, Z.B. Li, G.R. Han, Hydrothermal synthesis of lead zirconate titanate nearly free-standing nanoparticles in the size regime of about 4 nm, Crystal Growth and Design 9 (2009) 13–16.
[9] M. Klee, R. Eusemann, R. Waser, W. Brand, H. Vanhal, Processing and electrical-properties of $Pb(Zr_xTi_{1-X})O_3$ ($X=0.2$–0.75) films—comparison of metalloorganic decomposition and sol–gel processes, Journal of Applied Physics 72 (1992) 1566–1576.
[10] C. Liu, B.S. Zou, A.J. Rondinone, Z.J. Zhang, Sol–gel synthesis of free-standing ferroelectric lead zirconate titanate nanoparticles, Journal of the American Chemical Society 123 (2001) 4344–4345.
[11] M. Kamlah, Ferroelectric and ferroelastic piezoceramics—modeling of electromechanical hysteresis phenomena, Continuum Mechanics and Thermodynamics 13 (2001) 219–268.
[12] I.R. Abothu, S.-F. Liu, S. Komarneni, Q.H. Li, Processing of $Pb(Zr_{0.52}Ti_{0.48})O_3$ (PZT) ceramics from microwave and conventional hydrothermal powders, Materials Research Bulletin 34 (1999) 1411–1419.
[13] B.L. Newalkar, S. Komarneni, H. Katsuki, Microwave-hydrothermal synthesis and characterization of barium titanate powders, Materials Research Bulletin 36 (2001) 2347–2355.
[14] S.J. Qiu, H.Q. Fan, X.D. Zheng, $Pb(Zr_{0.95}Ti_{0.05})O_3$ Powders synthesized by pechini method: effect of molecular weight of polyester on the phase and morphology, Journal of Sol-Gel Science and Technology 42 (2007) 21–26.
[15] A. Abreu Jr., S.M. Zanetti, M.A.S. Oliveira, G.P. Thim, Effect of urea on lead zirconate titanate $Pb(_{Zr0.52}Ti_{0.48})O_3$ nanopowders synthesized by the pechini method, Journal of the European Ceramic Society 25 (2005) 743–748.
[16] S.M. Selbach, T. Tybell, M.A. Einarsrud, T. Grande, Size-dependent properties of multiferroic $BiFeO_3$ nanoparticles, Chemistry of Materials 19 (2007) 6478–6484.
[17] M.A. Zaghete, J.A. Varela, M. Cilense, C.O. Paiva-Santos, W.C. Las, E. Longo, The effect of isostructural seeding on the microstructure and piezoelectric properties of PZT ceramics, Ceramics International 25 (1999) 239–244.
[18] V.A. Chaudhari, G.K. Bichile, Structural and impedance spectroscopic studies on $PbZr_xTi_{1-X}O_3$ ceramics, Physica B 405 (2010) 534–539.
[19] M.L. Moreira, G.P. Mambrini, D.P. Volanti, E.R. Leite, M.O. Orlandi, P. S. Pizani, V.R. Mastelaro, C.O. Paiva-Santos, E. Longo, J.A. Varela, Hydrothermal microwave: a new route to obtain photoluminescent crystalline $BaTiO_3$ nanoparticles, Chemistry of Materials 20 (2008) 5381–5387.
[20] A.P. de Moura, R.C. Lima, M.L. Moreira, D.P. Volanti, J.W. M. Espinosa, M.O. Orlandi, P.S. Pizani, J.A. Varela, E. Longo, ZnO architectures synthesized by a microwave-assisted hydrothermal method and their photoluminescence properties, Solid State Ionics 181 (2010) 775–780.
[21] D.P. Volanti, M.O. Orlandi, J. Andres, E. Longo, Efficient microwave-assisted hydrothermal synthesis of CuO sea urchin-like architectures via a mesoscale self-assembly, CrystEngComm 12 (2010) 1696–1699.
[22] G.F. Teixeira, G. Gasparotto, E. Paris, M.A. Zaghete, E. Longo, J. A. Varela, Photoluminescence properties of PZT 52/48 synthesized by microwave hydrothermal method using PVA with template, Journal of Luminescence 132 (2012) 46–50.
[23] A.P. Singh, S.K. Mishra, D. Pandey, C.D. Prasad, R. Lal, Low-temperature synthesis of chemically homogeneous lead-zirconate-titanate (PZT) powders by a semi-wet method, Journal of Materials Science 28 (1993) 5050.
[24] S. Satapathy, V.K. Wadhawan, Fabrication of pyroelectric laser-energy meters and their characterization using Nd:Yag laser of variable pulse-width, Sensors and Actuators A 121 (2005) 576–583.
[25] C.L. Huang, B.H. Chen, L. Wu, Application feasibility of $Pb(Zr,Ti)O_3$ ceramics fabricated from sol-gel derived powders using titanium and zirconium alkoxides, Materials Research Bulletin 39 (2004) 523–532.
[26] J. Milanez, A.T. de Figueiredo, S. de Lazaro, V.M. Longo, R. Erlo, V. R. Mastelaro, R.W.A. Franco, E. Longo, J.A. Varela, The role of oxygen vacancy in the photoluminescence property at room temperature of the $CaTiO_3$, Journal of Applied Physics 106 (2009) (43526–43526-7).
[27] V.M. Longo, A.T. de Figueiredo, S. de Lazaro, M.F. Gurgel, M.G. S. Costa, C.O. Paiva-Santos, J.A. Varela, E. Longo, V.R. Mastelaro, F. S. De Vicente, A.C. Hernandes, R.W.A. Franco, Structural conditions that leads to photoluminescence emission in $SrTiO_3$: an experimental and theoretical approach, Journal of Applied Physics 104 (2008) (23515-23515-11).